Evidence for superelevation, channel incision, and formation of cyclic steps by turbidity currents in Eel Canyon, California

Michael P. Lamb*
Department of Earth and Planetary Science, University of California, Berkeley, California 94720-4767, USA

Jeffrey D. Parsons
Herrera Environmental Consultants, 2200 Sixth Avenue, Seattle, Washington 98121, USA

Beth L. Mullenbach
Department of Oceanography, Texas A&M University, College Station, Texas 77843-3146, USA

David P. Finlayson
School of Oceanography, University of Washington, Seattle, Washington 98195-7940, USA

Daniel L. Orange
University of California, Santa Cruz, California 95064, USA, and AOA Geophysics Inc., Moss Landing, California 95039; now at Black Gold Energy, Jakarta, Indonesia

Charles A. Nittrouer
School of Oceanography, University of Washington, Seattle, Washington 98195-7940, USA

ABSTRACT

We performed a multibeam survey of Eel Canyon, offshore northern California. The survey revealed a significant bend in the canyon that appears to be due to the oblique compressional tectonics of the region. A series of steps within a linear depression, ~280 m above the canyon floor, extends from the canyon rim at this bend to the subduction zone and a distinct fan-like topographic rise. We hypothesize that the linear depression is a distributary channel and the steps are cyclic-step bedforms created by turbidity currents. Our interpretation indicates that turbidity currents are able to run up and overspill the 280-m-high canyon wall, resulting in a partial avulsion of the canyon and the construction of a fan lobe that is offset from the canyon mouth. Simple hydraulic calculations show that turbidity currents generated in the canyon head from failure of 2–3 m of material would be capable of partially overflowing the canyon at this bend, assuming steady-uniform flow, full conversion of the failed mass into a turbidity current, and a range of friction coefficients. These estimates are consistent with analyses of sediment cores collected in the head of Eel Canyon, which suggest that 2–3 m of material fails on decadal time scales. Our calculations show that the overflowing parts of the currents would have large shear velocities (>10 cm/s) and supercritical Froude numbers, consistent with erosion of the distributary channel and formation of cyclic steps by turbidity currents.

Keywords: submarine canyons, Eel River, turbidity currents, cyclic steps, channel formation, superelevation, avulsion.

INTRODUCTION

Turbidity currents are considered to be the dominant mechanism for carving submarine canyons (Daly, 1936; Kuenen, 1937), yet the interactions between turbidity currents and the canyons they incise are poorly known. Stratigraphic models suggest that submarine canyons and their associated fans are most active during sea-level lowstands, when rivers' mouths are near the shelf-slope break and sediment loads are high (e.g., Stow et al., 1985; Posamentier et al., 1991). On collisional margins, however, canyons can be active conduits for sediment even during sea-level highstands due to the relatively narrow continental shelves and high sediment loads found there. For example, the head of Monterey Canyon, California, is currently near the mouth of the Salinas River, and turbidity currents occur frequently within the canyon (Johnson et al., 2001; Paull et al., 2003). In such settings, tectonics, sea level, climate, and sediment supply all play important roles in shaping submarine geomorphology (e.g., Orange, 1999; Burger et al., 2002). Understanding the interaction of turbidity currents with the evolving morphology of submarine canyons is necessary for predicting the morphodynamics of the canyons, as well as the stratigraphic evolution of the submarine fans that they feed.

While turbidity currents are analogous to rivers in many respects, they differ in important ways. Like rivers, turbidity currents are driven by their excess density over the ambient fluid. The density difference between a turbidity current and the surrounding seawater, however, is much less than the density difference between a river and the surrounding air. One important result of this is that turbidity currents are able to run up obstacles several times their flow depth through a process known as superelevation (Rottman et al., 1985; Muck and Underwood, 1990; Lane-Serff et al., 1995; Kneller and McCaffery, 1999). While superelevation has received considerable attention for understanding overbank deposition in meandering submarine-fan channels (Komar, 1969; Hay, 1987; Peakall et al., 2000; Pirmez and Imran, 2003) and overspill from enclosed minibasin topography (Pratson and Ryan, 1994; Edwards, 1993; Lamb et al.,

*E-mail: mpl@berkeley.edu

GSA Bulletin; March/April 2008; v. 120; 3/4; p. 463–475; doi: 10.1130/B26184.1; 12 figures.

2006), it is generally not considered for flows within incised canyons on the continental slope (Shepard and Dill, 1966). In fact, submarine canyons are considered to be the "type example of point sources turbidite systems" (Normark et al., 1993, p. 102), indicating that overspill is not thought to occur.

Herein we examine the interaction of turbidity currents with the topography of Eel Canyon, offshore northern California, based on a new bathymetric survey of the region. Eel Canyon is morphologically complex, which in part is due to the active tectonics of the region (Clarke, 1992). Of note is a large-scale ~90° bend in the canyon that turbidity currents must negotiate. In this paper we discuss a channel-like feature that extends outside of the canyon from this bend to the continental rise and a fan-like topographic feature. The floor of the channel is composed of long-wavelength quasi-periodic steps, which we interpret to be cyclic-step bedforms created by turbidity currents. We hypothesize that turbidity currents are capable of overflowing the canyon at the bend due to superelevation, and are responsible for incision of the distributary channel, formation of the cyclic steps, and construction of the fan lobe. We use simple hydraulic calculations to show that modern failures in the canyon head can produce turbidity currents capable of overflowing the canyon wall. Our interpretation is significant because it implies that turbidity currents can partially avulse deeply incised canyons and shift the locus of submarine fan deposition.

BACKGROUND

The Eel Canyon is located in the tectonically complex region of the Cascadia subduction zone and the Mendocino Triple Junction (MTJ) (Clarke, 1992) (Fig. 1). The region north of the MTJ is characterized by east-northeast compression related to the subduction of the Gorda plate beneath the North American plate. South of the MTJ, transpression associated with the San Andreas system dominates. The junction is migrating northward at an average rate of 64 mm/yr (Atwater, 1970; McCrory, 1989); this produces a zone of north-south compression extending ~80 km north of the MTJ (Burger et al., 2002; Gulick and Meltzer, 2002). The Eel Canyon is within the zone where the structural grain has been deformed in response to the migrating MTJ (Fig. 1). Burger et al. (2002) hypothesized that the Eel Canyon formed ca. 500 ka when arrival of the MTJ (Gulick and Meltzer, 2002) resulted in uplift-induced erosion and shelf bypass of sediment.

The Eel River basin has been the subject of recent work to connect terrestrial sediment sources to the resulting depositional record (Nittrouer and Kravitz, 1996; Nittrouer, 1999, Nittrouer et al., 2007). The Eel River is the primary source of sediment to the offshore basin and has exceptionally high sediment yields (~2 × 10^7 ton/yr) for its drainage area (~9400 km^2) (Griggs and Hein, 1972; Milliman and Syvitski, 1992). Much of the sediment discharged from the river during glacioeustatic and tectonic sea-level lowstands was probably funneled down Eel Canyon, as indicated by buried channels (formed between 363 and 300 ka) imaged on the present-day shelf (Burger et al., 2001). Currently, ~50% of the sediment discharged from the Eel River is deposited on the shelf and open slope, and the remaining 50% remains unaccounted for over decadal time scales (Sommerfield and Nittrouer, 1999; Crockett and Nittrouer, 2004; Alexander and Simoneau, 1999). It is likely that much of the missing modern sediment resides in or is funneled through Eel Canyon (Scully et al., 2003; Mullenbach and Nittrouer, 2006).

The upper Eel Canyon has been shown to be an active pathway for gravity-driven sediment transport over seasonal time scales. An instrumented tripod was deployed in the uppermost reaches of the canyon at 120-m water depth and documented the passage of a series of sediment-laden gravity currents (Puig et al., 2003; 2004). These events were generally not correlated with river discharge, and the gravity-driven transport was strongly influenced by wave motions. Though the gravity flows were not directly related to a particular flood event, surficial sediment found in the upper canyon was recently discharged from the river (on the order of days to months) based on short-time scale radioisotopic tracers found in cores (Mullenbach et al., 2004). Seasonal deposits reaching thicknesses greater than ten centimeters are common in cores from the canyon head following periods of elevated fluvial discharge. Most deposits are physically stratified, and some exhibit stratigraphic and radioisotopic discontinuities that point to the importance of slope failure over decadal time scales (Mullenbach and Nittrouer, 2006; Drexler et al., 2006).

Multibeam and multichannel seismic surveys of the Eel continental margin have been performed to understand how the overall structure of the region (Clarke, 1992; Orange, 1999; Gulick et al., 1998, 2002; Gulick and Meltzer, 2002) and the topography of the shelf (Goff et al., 1996; Burger et al., 2001) relate to the mid-shelf mud depocenter (Sommerfield and Nittrouer, 1999; Wheatcroft and Borgeld, 2000). Concurrent coring and multibeam surveys of the abyssal plain and rise complemented these earlier studies (Nelson et al., 2000). A survey focusing on Eel Canyon, however, was not performed. Owing to the newly appreciated importance of the canyon as a conduit for sediment (i.e., Mullenbach et al., 2004; Puig et al., 2004), we have mapped the canyon and identified features that we interpret to be evidence for turbidity currents.

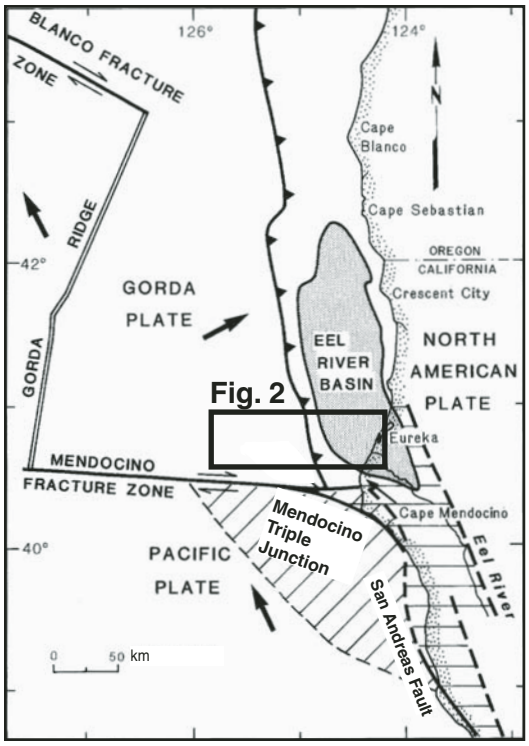

Figure 1. Regional map of offshore northern California showing major plate boundaries (after Clarke, 1992). The box roughly outlines the area shown in Figure 2.

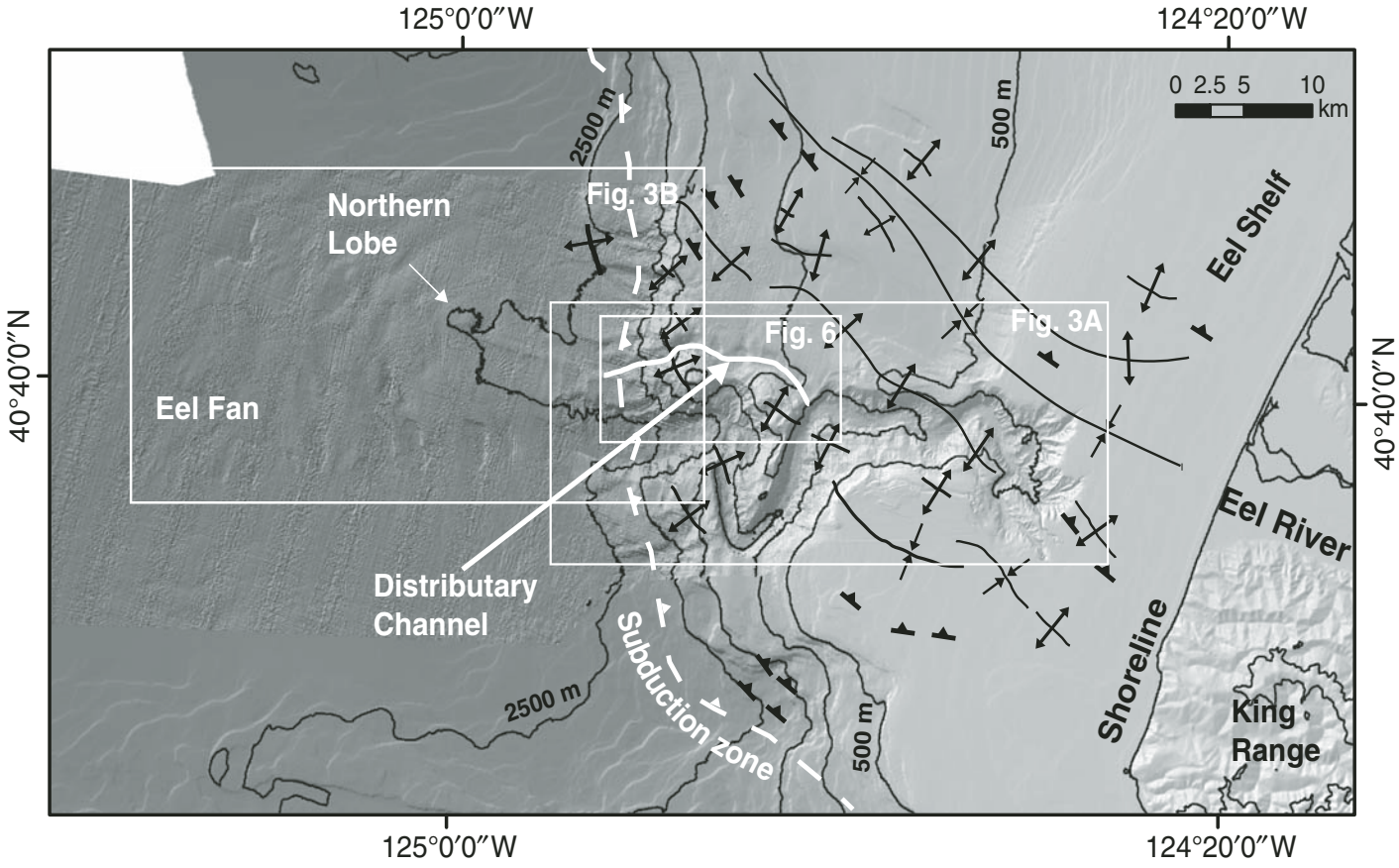

Figure 2. Bathymetric and topographic map of the surveyed and surrounding area. The hillshade has no vertical exaggeration and the sun angle is from the northwest. The new surveyed area extends from the head of Eel Canyon to the western border of the image and has a resolution of 10 m. This data set overlays previously collected bathymetric and topographic data with a resolution of 78 m (Divins and Metzger, National Geophysical Data Center Coastal Relief Model, http://www.ngdc.noaa.gov/mgg/coastal/coastal.html). The new survey appears rougher than the previous data set because of the difference in resolution and because the new data set has not been smoothed. The structural interpretations follow Clarke (1992), based on bathymetric and seismic surveys. The thin black lines are topographic contours with a 500-m contour interval. The white boxes show the locations of Figures 3A, 3B, and 6 (datum: WGS 84; projection: Universal Transverse Mercator zone 10N).

BATHYMETRY OF THE EEL CANYON

We obtained bathymetry by using the Krupp Atlas Elektronik Hydrosweep system aboard the R/V *Thomas G. Thompson* in mid-October of 2001. The nominal echo frequency of the Hydrosweep is 15.5 kHz, with 59 beams spread throughout 90°. The outer beams were subject to large error associated with cross-contamination between beams (particularly in areas of rough topography) and variability in the speed of sound calculation. As a result, we truncated the outer 1–5 beams, depending on the degree of overlap with adjacent lines. The result is an along-track artifact (rail or seam) that appears at the junction between adjacent swaths. Considering that the topography of the canyon is extremely rough, we have not spatially filtered the output to eliminate the along-track artifact.

The survey mapped Eel Canyon from its head westward across the subduction zone and the Eel Fan (also known as the Gorda Fan) (Figs. 1 and 2). The head of the canyon is located ~10 km landward of the shelf-slope break and ~10 km seaward of the present-day shoreline and the mouth of the Eel River (Fig. 2). The canyon is composed of four reaches, numbered 1–4 for the purpose of comparison, joined at significant bends (Fig. 3A). The canyon terminates at the subduction zone (as mapped by Clarke, 1992) where the Eel Fan has been constructed (Figs. 2 and 3B).

To illustrate the morphology of the canyon, we have constructed cross sections and profiles for each reach, the locations of which are shown in Figure 3. The longitudinal profile along the canyon floor was determined from a digital elevation model (DEM) following the steepest-slope path (Jenson and Domingue, 1988; Martz and Garbrecht, 1998). From near the canyon head to ~1.7 km depth, corresponding to reaches 1, 2, and part of 3, the profile of the canyon floor is approximately linear with a slope of 2.6% (calculated using a linear least-squares fit) (Fig. 4). At ~1.7 km depth (midway down reach 3), the slope increases abruptly to ~13.5% until ~2.5 km depth, where it shallows within reach 4 near the mouth of the canyon.

The canyon is approximately V-shaped in cross section with a relatively narrow thalweg (Fig. 5). This geometry is similar to that of other active-margin submarine channels (Hagen et al., 1996). Reach 4, however, is more U-shaped in cross section than the rest of the canyon. Greene et al. (2002) also observed a down-canyon change from V-shaped to U-shaped cross sections in the morphology of Monterey Canyon. They attributed the change to a lithofacies boundary between continental crust and

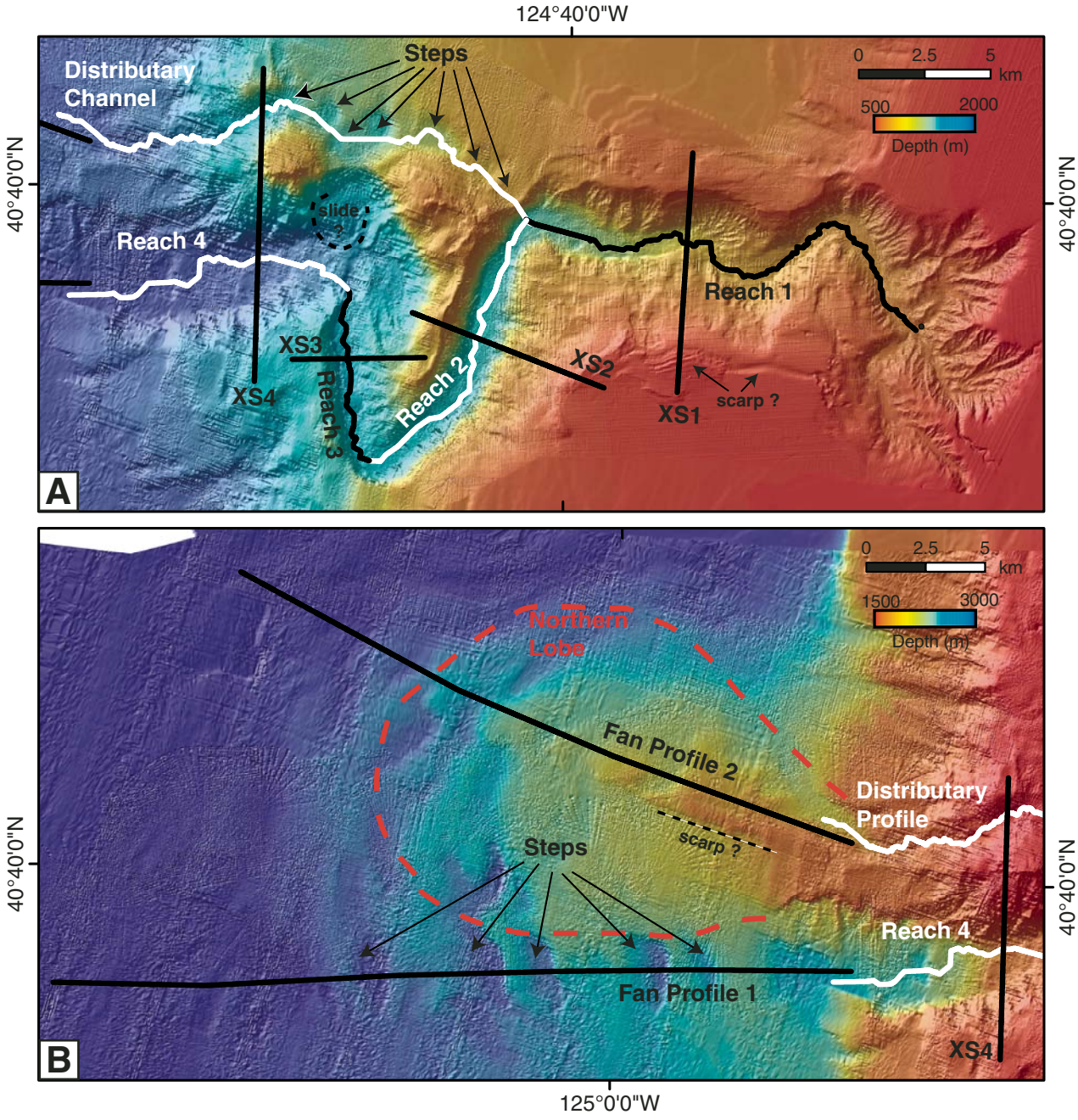

Figure 3. Bathymetric maps of the Eel Canyon and Eel Fan. The hillshade has no vertical exaggeration and the sun angle is from the northwest. The colors represent elevations; however, the color scheme is nonlinear and has been skewed to highlight key features. The geographic locations of the maps are shown in Figure 2. (A) The longitudinal profiles for the four reaches were found by routing flow down the path of steepest decent. The profiles are shown in Figure 4. The four cross sections (labeled XS1, XS2, XS3, and XS4) are shown in Figure 5. The locations of the steps and the distributary channel are also shown, and the corresponding profiles are given in Figure 4. (B) Bathymetric map of the Eel Fan and the northern lobe. The fan profiles are shown in Figure 8. Note that the color bar and scale bar are different in A and B (datum: WGS 84; projection: Universal Transverse Mercator zone 10N).

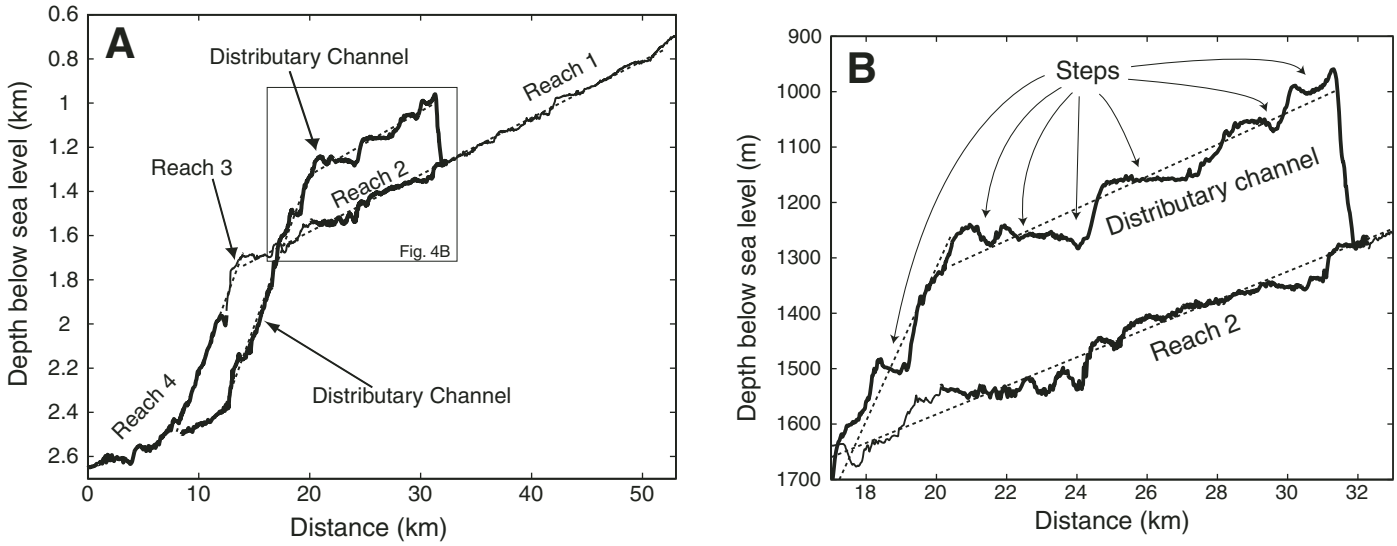

Figure 4. (A) Longitudinal profiles of the four reaches of the canyon and the distributary channel. The solid lines represent the actual data extracted from the digital elevation model, as shown in Figure 3. The lines alternate thick and thin to differentiate between reaches. The dashed lines are linear fits to the profiles used to estimate slope. The canyon floor has a slope of ~2.6% from a distance of ~12 to 55 km, and a slope of ~13.8% from 5 to 12 km. The distributary channel has an average slope of 2.9% between 20 km and 31 km, and 13.8% between 12 km and 20 km. (B) Detail of profiles showing the locations of the steps. See Figure 6 for a plan view of the steps. Some of the small-scale roughness is due to the spatial resolution of the data (10 m).

accretionary-wedge sediments. The landward edge of reach 4 roughly corresponds with the transition to the toe of the accretionary complex described by Orange (1999).

The cross section of the canyon is generally asymmetric with steeper sloping canyon walls on one side. For example, the right wall (when facing downstream) has slopes of 45%, 43%, 42%, and 48%, while the left wall has slopes of 25%, 30%, 50%, and 23% for reaches 1–4, respectively. These slopes were calculated using a linear-least-squares fit to the cross sections shown in Figure 5 (XS1, XS2, XS3, and XS4), the locations of which are shown in Figure 3. The steeper dipping walls generally correspond to the outer banks of the three major bends in the canyon. The right bank is the outer bank for reaches 1, 2, and 4, and the left bank is the outer bank for reach 3. This correlation is expected because gravity currents (e.g., turbidity currents or rivers) tend to move faster and are more erosive along their outer banks.

The steeper sloping canyon walls appear to be rougher and more gullied than the shallower sloping walls. For example, the north (right bank) wall of reach 1 is steep and gullied, while the south wall appears hummocky, and several small landslide scarps and deposits are visible (Fig. 3A). The south wall of reach 1 is also bounded by a canyon-parallel scarp near the canyon rim, which is similar to those observed on the Atlantic continental margin that are associated with large slides (Driscoll et al., 2000). A potential slide deposit visible along the north wall of reach 4 has an estimated area in excess of 3 km^2 (Fig. 3A).

The major morphologic features of the canyon are the large bends that separate the four reaches. Given the transpressional tectonics of the region, it is likely that the bends have been influenced by deformation. For example, the location of reach 3 is coincident with anticlines, as mapped by Clarke (1992) (Fig. 2). This region also is coincident with the landward edge of trench-parallel folds and thrusts, described by Orange (1999) as the accretionary toe—a region typified by dramatic shortening and significant tectonic distortion due to the subducting Gorda plate. The crest of the west wall halfway down reach 2 intersects an anticline (Fig. 2), and is significantly higher (>200 m) than any other point mapped on the continental margin at any equivalent distance seaward (Fig. 3).

Of particular interest for this paper is a linear channel-like depression (referred to as a channel herein for brevity) that emanates from the 90° bend in the canyon axis at the junction of reaches 1 and 2, and extends to a fan-like topographic rise (referred to as the northern lobe) (Figs. 2 and 3). Figure 6 shows a detailed topographic map of this channel. The axis of the channel intersects the west wall of reach 2 approximately 280 m above the canyon floor. At this location, the rim of the west wall of reach 2 is at its lowest elevation. The channel appears to initially follow the northwest grain of a series of anticlines as mapped by Clarke (1992) but becomes increasingly oblique to these features near the subduction zone (Fig. 2). The longitudinal profile of the channel (following the path of steepest descent) has an overall slope of 2.9% (using a linear least-squares fit), which is similar to the slope of ~2.6% of the canyon floor in reaches 1 and 2 (Fig. 4). Like the main canyon (and the regional topography), there is an abrupt increase in slope to 13.8% near the subduction zone (Fig. 4).

The channel profile is not smooth but is composed of a series of seven steps (Fig. 4B). In plan view, these steps appear as quasi-circular topographic depressions within the channel (Fig. 6). The steps have a wavelength of ~2 km and a typical height of 100 m within the 2.9% sloping reach. At approximately the same distance seaward, the main canyon floor within reach 2 also appears to be composed of a series of steps, although these are not as distinct as the steps in the channel (Fig. 4B).

Figure 7 shows three cross sections of the channel and steps (DXS1, DXS2, DXS3), the locations of which are shown in Figure 6. The cross-sectional relief of the channel (i.e., the height of the channel sidewalls) is typically 100 m within the 2.9% grade reach but can be as great as 150 m within a step and ~50 m in between steps (Fig. 7). The floor of the channel

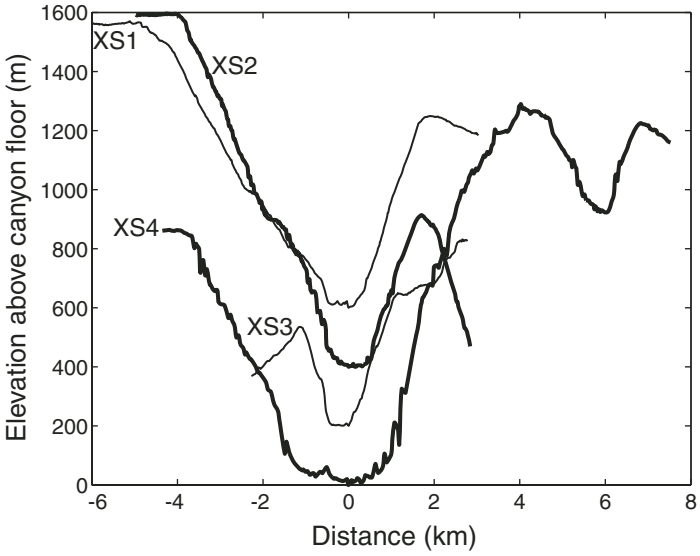

Figure 5. Cross sections of Eel Canyon. The locations of the sections are shown in Figure 3A. All cross sections have been orientated so that the view is looking downstream (i.e., the left side of the figure corresponds to the left bank of the canyon). The elevation is relative to the lowest point along the canyon floor for each cross section. The x-axis is the distance relative to the center of the canyon, which is defined as the location along the cross section with the lowest elevation. Cross sections XS1, XS2, and XS3 are shifted upward by 300 m, 200 m, and 100 m, respectively, for clarity. Note that the right most part of XS4 crosses the distributary channel (see Fig. 6).

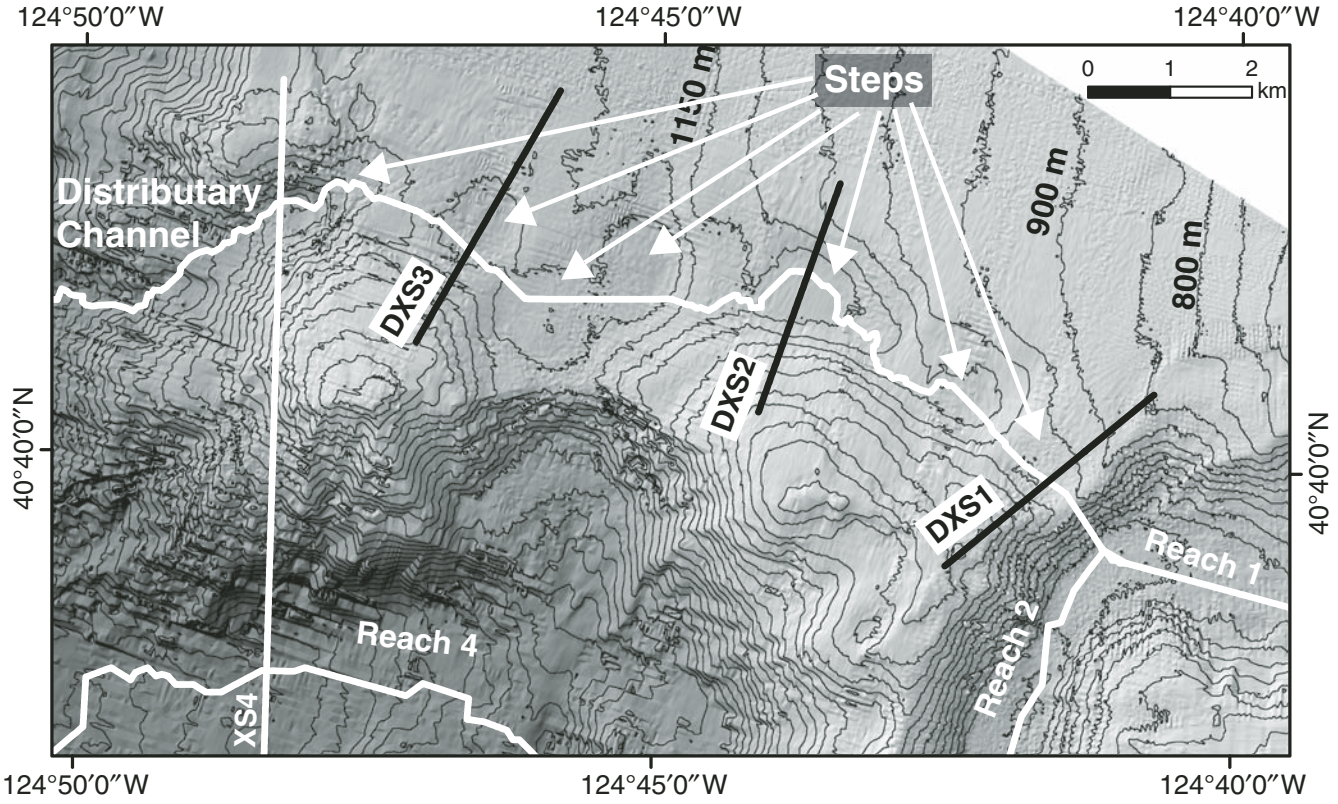

Figure 6. Bathymetric map of the distributary channel and steps. The geographic location of the map is given in Figure 2. The hillshade has no vertical exaggeration, and the sun angle is from the northwest. The black lines are topographic contours with a contour interval of 50 m. Much of the small-scale roughness along contour is due to the spatial resolution of the data (10 m). The longitudinal profiles (following the path of steepest descent) of the distributary channel, reaches 1, 2, and 4, and cross section 4 (XS4) are shown by white lines. Cross sections of the distributary channel (DXS1, DXS2, and DXS3) are shown by black lines and are given in Figure 7. Note that the steps appear as quasi-circular depressions in plan view (datum: WGS 84; projection: Universal Transverse Mercator zone 10N).

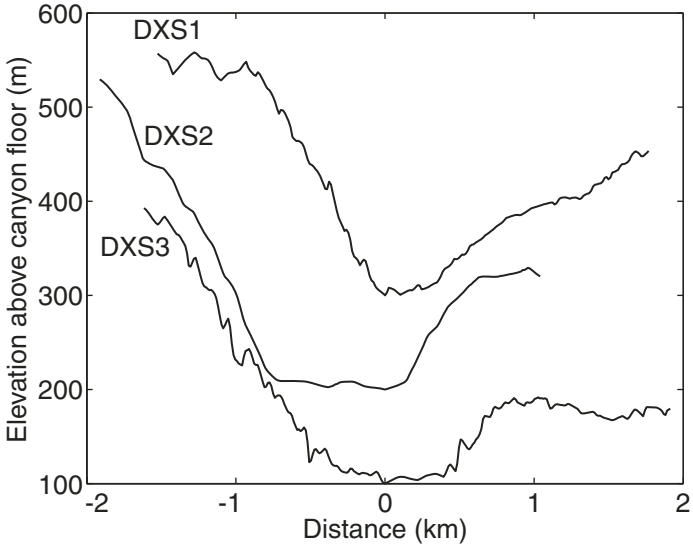

Figure 7. Cross sections of the distributary channel, the geographic locations of which are shown in Figure 6. All cross sections have been orientated so that the view is looking downstream (i.e., the left side of the figure corresponds to the left bank of the channel). The elevation is relative to the lowest point along the channel floor for each cross section. The x-axis is the distance relative to the center of the channel, which is defined as the location along the cross section with the lowest elevation. Cross sections DXS1 and DXS2 are shifted upward by 200 m and 100 m, respectively, for clarity.

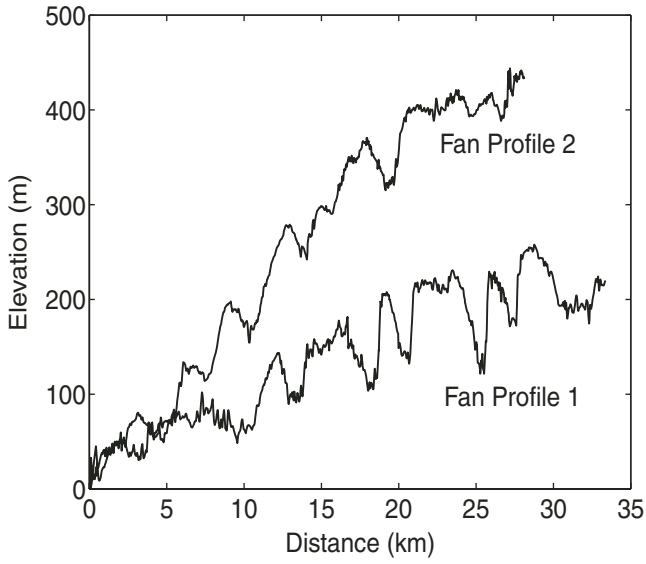

Figure 8. Longitudinal profiles across the Eel Fan and the northern lobe. The locations of the profiles are shown in Figure 3B. The elevations and distances are relative to the distal point of each profile. The fan surfaces have average slopes of 0.64% and 2.1% for fan profiles 1 and 2, respectively, using a linear least-squares fit.

is relatively flat and 500–1000 m wide, with a trend of increasing width downstream. Cross section 4 of the main canyon (XS4; Fig. 5) extends across the smaller channel downslope of the major slope break. This profile shows that the channel has ~300 m of cross-sectional relief on the steeper 13.8% grade. The channel is bordered to the south (left bank when facing downstream) by a topographic rise, and the channel walls on this side are generally steeper than the right bank. For example, the left-bank walls for cross-sections DXS1, DXS2, and DXS3 have slopes of 30%, 23%, and 25%, respectively, while the right-bank walls have slopes of 8%, 21%, and 20% (Fig. 7).

Directly seaward from the mouth of the canyon is the Eel Fan (Figs. 2 and 3B). It is interesting that the main topographic rise of the fan does not appear to be associated spatially with the mouth of the canyon. Instead, this northern lobe is north of the canyon mouth and in line with the smaller channel described above (Fig. 3B). Near the apex of the northern lobe there is a linear scarp-like feature (Fig. 3B), which suggests that some of the local relief might be tectonically induced. A series of wave-like steps also occur directly seaward of the canyon mouth and across northern lobe (Fig. 8). These features have a height of ~50–100 m and a wavelength of ~2.8 km on an overall slope of 0.64% for fan profile 1 and 2.1% for fan profile 2.

EVIDENCE FOR TURBIDITY CURRENTS

The waves on the northern lobe are similar to sediment-wave bedforms found on other submarine fans (e.g., Monterey Fan, California; Fildani and Normark, 2004), which are thought to occur under depositional turbidity currents. The series of steps in the small channel are similar to cyclic-step bedforms found in bedrock rivers (e.g., Wohl, 2000) and flume experiments with cohesive and erodible beds (Sawai, 1977; Koyama and Ikeda, 1998). Fildani et al. (2006) argued that features on the submarine Monterey Fan, California, are analogous to subaerial cyclic steps but carved by turbidity currents rather than rivers. Like the Eel Canyon, a channel with periodic steps is located on the Monterey East Channel where the flow is forced through a significant bend, Shepard meander. The Monterey cyclic steps are larger than those on the Eel Canyon (by about a factor of two in wavelength and step height), but the aspect ratio is similar.

Fortunately, theories have been developed for cyclic steps over a cohesive or bedrock bed (Parker and Izumi, 2000) and over an alluvial bed (Sun and Parker, 2005; Taki and Parker, 2005) by rivers and turbidity currents (Kostic

and Parker, 2006). This work indicates that cyclic steps occur in Froude-supercritical flows ($Fr_d > \sim 1$), which are expected for turbidity currents in steep canyon systems. The bulk densimetric Froude number is defined as

$$Fr_d = \frac{U}{\sqrt{RCgh}} \quad (1)$$

where U is the depth-averaged velocity, C is the depth-averaged volumetric sediment concentration, R is the submerged specific gravity of the sediment (~1.6), g is the gravitational acceleration (9.8 m/s^2), and h is the flow depth. Figure 9 shows an illustration of self-formed cyclic steps (following Parker and Izumi, 2000). The flow accelerates and becomes supercritical ($Fr_d > 1$) over a step. At the base of the step, a hydraulic jump ($Fr_d = 1$) forms, and the flow is subcritical downstream of the jump ($Fr_d < 1$). Acceleration then occurs over the next step and the process continues. Over an erodible bed, the steps are stable and migrate upstream.

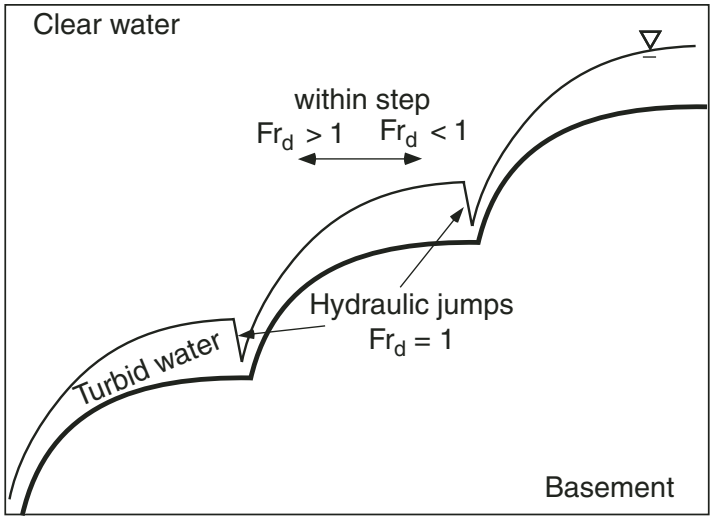

Figure 9. Illustration of cyclic steps formed by a turbidity current (modified from Parker and Izumi, 2000). Fr_d in the schematic is local densimetric Froude number.

The drainage-network algorithm used to generate the channel and canyon profiles shown in Figure 4 (Jenson and Domingue, 1988; Martz and Garbrecht, 1998) indicates that a gravity current capable of overflowing the 280-m wall at the 90° bend in the canyon (at the junction of reaches 1 and 2) would flow downslope, through the channel-like depression, and to the northern lobe of the submarine fan (Fig. 3). This suggests that this linear depression could be a distributary channel that serves as a conduit for turbidity currents. This interpretation explains why the depression is parallel to the trend of the regional slope (i.e., the direction gravity currents would flow), nearly the same slope as the main canyon, along strike with reach 1 of the main canyon, bounded upstream by a major bend in the canyon (where one might expect superelevation and overspill of turbidity currents), and bounded downstream by the apex of the northern lobe. Furthermore, the presence of steps in the channel is consistent with cyclic-step bedforms generated by turbidity currents.

Nonetheless, without direct observation (e.g., core samples or seismic-reflection profiles) it is difficult to rule out a tectonic origin for some of these features. Tectonics have likely played a role in deforming the canyon and creating the abrupt bends. It seems unlikely, however, that the 90° bend in the canyon, the linear channel-like depression, the quasi-periodic steps, and the northward displaced fan all were created and coincidently aligned by tectonic deformation. In contrast, these features would be expected from erosion and deposition by turbidity currents.

The morphologic features described herein do not resolve the origin of the turbidity currents forming the canyon or the distributary channel. The cyclic steps imply that flow was sustained long enough for setup of periodic hydraulic jumps. This suggests flow durations of tens of minutes or more (e.g., Lamb et al., 2004a). One possible generation mechanism is plunging hyperpycnal river plumes (Nemec, 1995; Mulder et al., 1997; Kineke et al., 2000; Parsons et al., 2001, 2007; Walsh and Nittrouer, 2003; Myrow et al., 2006). Hyperpycnal plumes were probably more common at sea-level lowstand because the Eel River would have fed directly into the canyon (Burger et al., 2001). Modeling efforts suggest, however, that large floods of the Eel River can produce hyperpycnal plumes during sea-level highstand as well (Mulder and Syvitski, 1995).

Nonetheless, oceanographic measurements indicate that Eel River floods and transport events in the canyon are generally not correlated in time (Puig et al., 2003). Much of the sediment discharged from the river is deposited on the inner and middle shelf (e.g., Wheatcroft and Borgeld, 2000; Crockett and Nittrouer, 2004), and some of this sediment is later suspended and moved seaward by wave-supported gravity currents (i.e., fluid muds) (e.g., Ogston et al., 2000; Traykovski et al., 2000, Scully et al., 2003). Laboratory experiments in a wave duct have shown that waves typical of the Eel continental shelf during storms are capable of supporting near-bed suspensions with depth-averaged concentrations of 25 kg/m^3 and high sand contents (up to 80%) (Lamb et al., 2004b; Lamb and Parsons, 2005). Gravity flows in the uppermost part of the canyon also have been attributed to failure of recently deposited material due to wave loading (Puig et al., 2004). Both wave-supported gravity currents and wave-induced failures probably contribute to the seasonal deposits in the canyon heads, which can be many centimeters thick, physically stratified, and in some cases contain high concentrations of sand (up to 50%) (Drexler et al., 2006). It is failure of these deposits on decadal time scales (Mullenbach and Nittrouer, 2006) that probably forms turbidity currents large enough to traverse the lower canyon, superelevate at the 90° bend in the canyon, overflow the 280-m-high canyon wall, carve the distributary channel, and form the cyclic steps. In the following section we test this hypothesis by using simple fluid-mechanical arguments to illustrate conditions necessary for overflow at the canyon bend.

ANALYSIS

To determine the size and speed of turbidity currents that might occur in the canyon, the amount of sediment contained within the flows needs to be established. Mullenbach and Nittrouer (2006) found that, at 160-m and 200-m water depth in the canyon head, ~2–3 m of sediment could fail about every 10–30 yr. These results were derived from the seasonal deposition rate, a stability analysis of the sediment accumulating on a fixed surface, and observed erosional contacts. The sharp contacts (evident from X- radiographs) were found to be coincident with down-core discontinuities in ^{210}Pb activity at some thalweg locations; this indicates that a significant portion of the sediment record had been removed. The failed material obtained from this analysis can be used as a one-dimensional estimate for the amount of sediment participating in a turbidity current.

The thickness of a turbidity current h can be calculated from continuity as

$$h = f(1-\phi)\eta / C \,, \qquad (2)$$

where f is the fraction of failed mass that participates in the turbidity current, η is the thickness of sediment to fail, and ϕ is the porosity of the seabed (0.65, which is consistent with core data). The sediment concentration of a turbidity current (i.e., its driving force) must be within a relatively small range and is typically ~20 kg/m^3 (i.e., $C \approx 0.75\%$; Parsons and Garcia, 1998). Flows that are substantially more concentrated (i.e., >100 kg/m^3) generally do not behave as a Newtonian fluid. Less concentrated flows (<10 kg/m^3) do not produce enough shear and turbulence to maintain the suspension. Unfortunately, the fraction of a failed mass that can become a turbidity current is poorly known. To proceed, we simply assume that all of the failed mass participates in the turbidity current ($f = 1$), making our estimate of h a maximum. This assumption is discussed in detail in the next section. Figure 10A shows the calculated maximum flow depth from equation 2 as a function of failure thickness, assuming $C = 0.75\%$ and $f = 1$. For a failed mass that is typical of the upper Eel Canyon (~2–3 m; Mullenbach and Nittrouer, 2006), the height of the current is calculated to range from 93 to 140 m. Note that this is significantly smaller than the height the flow must achieve to overflow the 280-m-high canyon wall at the bend between reaches 1 and 2.

There are two mechanisms that might explain how turbidity currents generated from failure of 2–3 m of material can overflow the 280-m-high canyon wall. First, turbidity currents can erode sediment from the bed and entrain ambient seawater. This can cause flows to grow large and fast due to a feedback between sediment entrainment and flow depth (or velocity) (Parker, 1982). The growth of a turbidity current due to entrainment, however, is difficult to quantify without introducing substantial assumptions (e.g., the erodibility of the bed). This effect, therefore, is neglected in our analysis, making our estimates of current height somewhat conservative.

The second mechanism is superelevation, which is expected for turbidity currents (or any gravity current) where the flow is directed around a bend or confronted by an obstacle (e.g., see Hay [1987] for a documented field case of turbidity-current superelevation). Turbidity currents superelevate because of the conversion of kinetic to potential energy, which allows them to abandon a confining channel or flow over an obstruction (e.g., Edwards, 1993; Lane-Serff et al., 1995; Kneller and Buckee, 2000; Lamb et al., 2004a). In order to estimate the magnitude

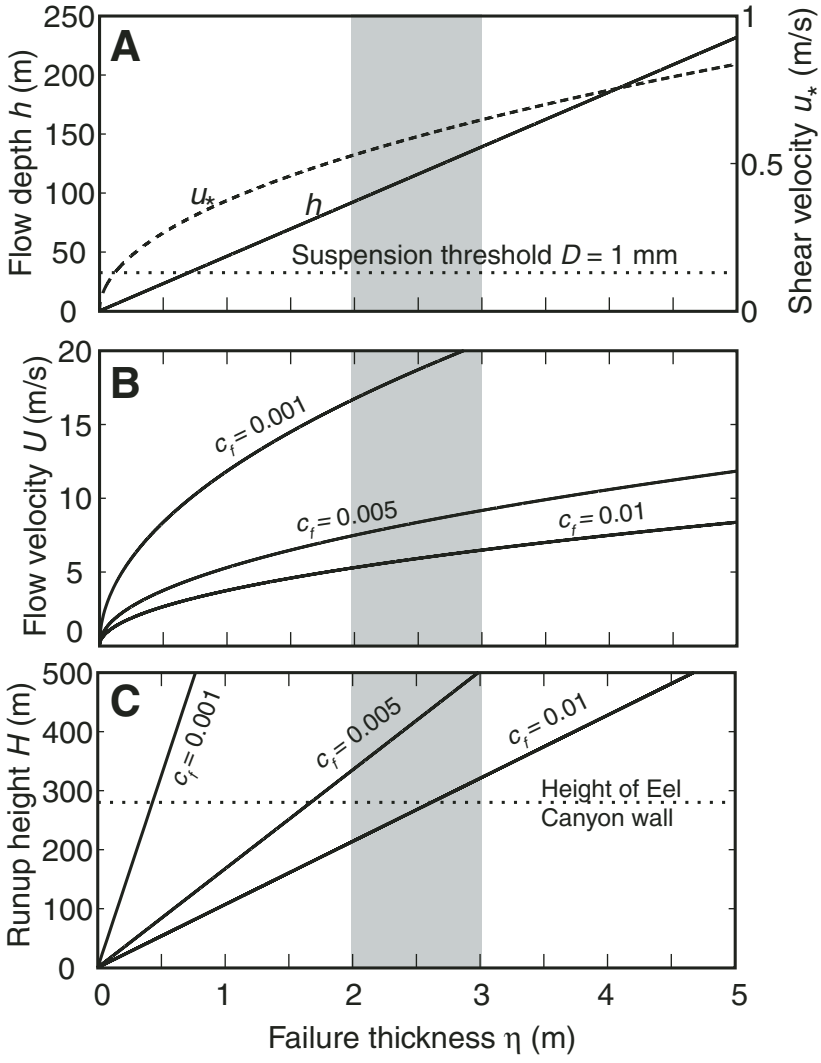

Figure 10. Estimates of turbidity-current characteristics within reach 1 (S = 2.6%) as a function of thickness of a failed mass (η). These calculations assume that 100% of the failed mass is converted into a turbidity current. The shaded region represents the size of failures that occur on decadal time scales in Eel Canyon, following the analysis of Mullenbach and Nittrouer (2006). (A) The flow depth h (solid line) calculated from equation 2 and bed shear velocity u_* (dashed line) calculated from equation 4 for various failure thicknesses. The horizontal dashed line represents the shear velocity necessary to suspend 1-mm-diameter (D) sediment. This was found by equating the shear velocity to the particle-settling velocity calculated for natural sediment following Dietrich (1982). (B) The depth-averaged flow velocity (U) of a turbidity current, calculated from equation 3, as a function of failure thickness for three different values of the friction coefficient (c_f). (C) The total runup height (H) of a turbidity current calculated from equation 5 for a range of failure thicknesses and friction coefficients. The height of the canyon wall at the junction of reaches 1 and 2 is shown as a dashed line for reference.

of superelevation, the velocity of the current first must be established.

For dilute turbidity currents (i.e., $C \ll 1$), the depth-averaged velocity U can be estimated by assuming steady and uniform flow conditions, as

$$U = \sqrt{u_*^2 / c_f} \ . \quad (3)$$

The bed shear velocity u_* is given by

$$u_* = \sqrt{RCghS} \ , \quad (4)$$

where S is the bed slope (where a low-slope approximation has been used: $\sin\theta \approx \tan\theta$) and c_f is a coefficient of friction that accounts for bed and entrainment drag along the boundaries of the current. The friction coefficient has been shown to range from 10^{-3} to 10^{-2} (Parker et al., 1987) although $c_f \approx 5 \times 10^{-3}$ is typically considered accurate for field-scale turbidity currents (e.g., Parker et al., 1986; Dade et al., 1994; Mulder et al., 1997; Pirmez and Imran, 2003). Because c_f is poorly known, we solve equations 3 and 4 for a range in friction coefficients as shown in Figure 10B. This, for example, results in a flow velocity ranging from 5.3 to 16.8 m/s for flow through reach 1 (S = 2.6%) generated from a 2-m-thick failure. This velocity is somewhat smaller than the calculations made by Heezen and Ewing (1952) of the turbidity current associated with the Grand Banks slide, but it is comparable to estimates for smaller turbidity currents in canyons and fan channels (e.g., Monterey East Channel: Fildani et al., 2006; Scripps Canyon: Inman et al., 1976; Amazon Fan: Pirmez and Imran, 2003).

Our calculated shear velocities u_* (Fig. 10A) are large, suggesting that the flows considered would be able to suspend sediment. Flows typically are considered competent to suspend sediment if the shear velocity is greater than the fall velocity of sediment w_s (i.e., $u_* > w_s$). For reference, Figure 10A shows the settling velocity for 1-mm sand, which is substantially larger than that for the unconsolidated mud or very fine sand typical of the upper canyon (Mullenbach and Nittrouer, 2006; Drexler et al., 2006). This supports the idea that our estimates of flow thickness and velocity are conservative because we have neglected the potential for flows to grow by entrainment of bed sediment.

The magnitude of superelevation can be estimated by balancing the centrifugal force and the resulting pressure gradient force in a bend (e.g., Komar, 1969; Pirmez and Imran, 2003). Recent experiments, however, have shown that this method substantially underestimates superelevation of turbidity currents: Straub et al. (2008) found more success by assuming full conversion of kinetic to potential energy, which is a common way to assess the overflow of obstacles by turbidity currents (e.g., Rottman et al., 1985; Muck and Underwood, 1990; Kneller and McCaffery, 1999). Therefore, we estimate the potential runup height of a turbidity current (H) as the sum of the current height and the magnitude of superelevation, assuming full conversion of kinetic to potential energy,

$$H = h + \frac{U^2}{2RCg} \ . \quad (5)$$

For all of the conditions considered, a 3-m failure would produce a flow capable of overflowing the 280-m-high canyon wall at the junction of reaches 1 and 2 (in some cases by hundreds of meters) (Fig. 10C). A 2-m failure would overflow the canyon at the bend as long as $c_f <\sim 7 \times 10^{-3}$, which is likely. While these estimates are crude, they nonetheless illustrate that it is plausible for modern failures in the head of Eel Canyon to produce turbidity currents capable of partially avulsing the canyon due to superelevation.

Because overspill of turbidity currents into the distributary channel seems possible, it is worth considering the flow conditions that might be prevalent there. Using the overall slope within the upper part of the distributary channel (S = 2.9%) and assuming C = 0.75%, we calculated the flow velocity and shear velocity (using equations 3 and 4) for a range in overflow depths and friction coefficients. From the estimates of runup, it seems likely that the overspilling turbidity currents would have flow depths of tens of meters or more (Fig. 10C). For these conditions, the calculated shear velocities are large in comparison with the competency thresholds for suspension of unconsolidated sand or mud (Fig. 11). Like the estimates for the main canyon, the calculated flow velocities in the distributary channel are meters per second or more (Fig. 11).

Equations 1–4 can be combined to estimate the bulk densimetric Froude number for the flows within the main canyon and in the distributary channel. Combining these equations shows that for steady uniform flow, the Froude

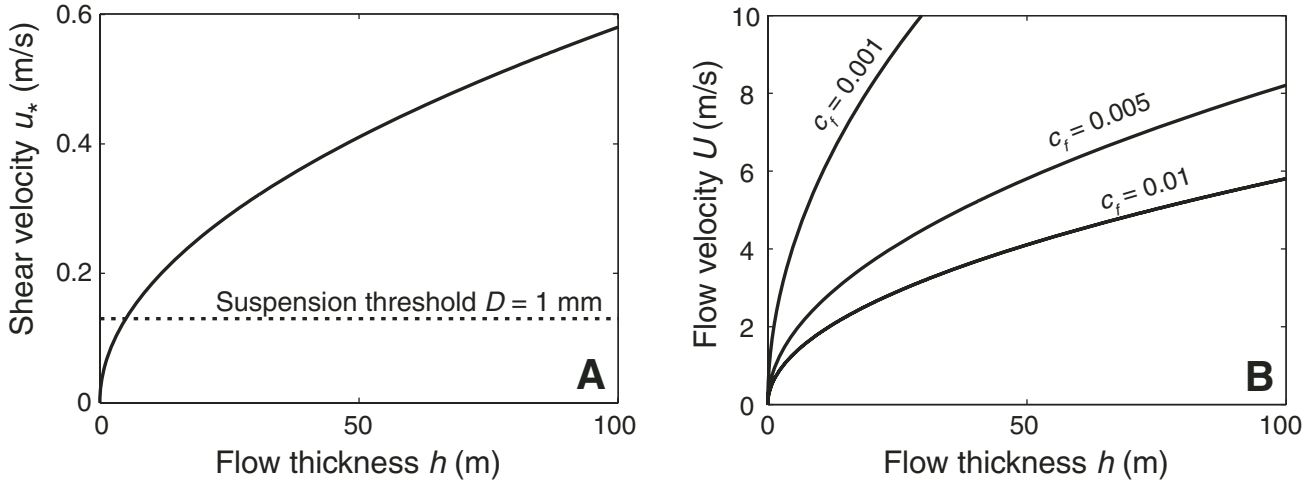

Figure 11. Estimates of turbidity-current characteristics within the distributary channel (S = 2.9%) as a function of thickness of the overflowing turbidity current (h). (A) The bed shear velocity u_* was calculated from equation 4. The horizontal dashed line represents the shear velocity necessary to suspend 1-mm-diameter (D) sediment (see Fig. 10 for details). (B) The depth-averaged flow velocity (U) of a turbidity current, calculated from equation 3), for three different values of the friction coefficient (c_f).

number is simply a function of the channel slope and the friction coefficient, i.e.,

$$\mathrm{Fr_d} = \frac{U}{\sqrt{RCgh}} = \sqrt{\frac{S}{c_f}}\,. \qquad (6)$$

For slopes >1%, supercritical Froude numbers are expected for all friction coefficients considered (Fig. 12). Given that the slopes in both the main canyon and the distributary channel exceed 1% by nearly a factor of three or more indicates that turbidity currents that occur there would be supercritical. This is consistent with our hypothesis that turbidity currents are responsible for formation of the cyclic steps, because cyclic steps require supercritical flow conditions (Parker and Izumi, 2000).

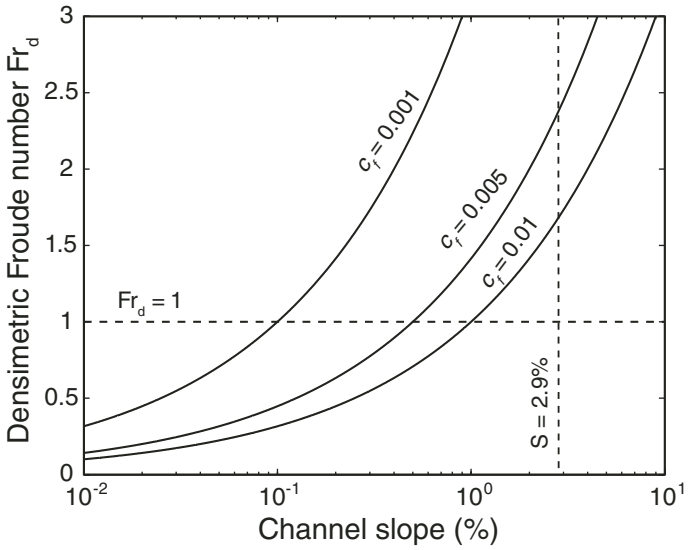

Figure 12. The bulk densimetric Froude number ($\mathrm{Fr_d}$) calculated from equation 6 as a function of channel slope (S) and the friction coefficient (c_f). The horizontal dashed line represents ($\mathrm{Fr_d}$) = 1, which is a minimum value needed for formation of cyclic steps. The vertical dashed line represents the average slope of the distributary channel (S = 2.9%). Note that all flows considered within the distributary channel would be supercritical and therefore capable of forming cyclic steps.

DISCUSSION

Perhaps the biggest limitation in our quantitative analysis of turbidity currents is the assumption of full conversion of a failed mass into a turbidity current. Because natural events are extremely destructive to any sort of equipment, most of the estimates of the efficiency of failures to produce turbidity currents have been based upon laboratory experiments (e.g., Mohrig et al., 1998; Marr et al., 2001). In the experiments analyzed by Mohrig and Marr (2003), ~1% of a failed mass was converted into a turbidity current. There are two key differences between previous experiments of slide-induced turbidity currents and the failures within the Eel Canyon. First, the sand contents typically examined in the laboratory experiments were much higher and the porosities were much lower than those found within the canyon. The individual beds found within Eel Canyon are predominantly silty with highly variable sand contents (0%–50%). The sand contents averaged over 30-cm-long cores are generally <20%, however, and the porosities are typically 0.65 or greater (Drexler et al., 2006). The experiments analyzed by Mohrig and Marr (2003) used mixtures that were predominantly sandy (48%–96%) with low porosities (0.34–0.53), and therefore were less easily sheared and mixed into turbidity currents. Second, and probably most important, is that mixing processes responsible for incorporation of failed material into a turbulent continuum are highly scale dependent (Parsons and Garcia, 1998). The addition of a large amount of sediment to the water column increases the effective viscosity of the flow, which in turn reduces the spectral gap between the large-scale mean motions of the flow and those associated with viscosity. The result is that fully turbulent behavior is extremely difficult to attain from a slope failure in any small-scale laboratory experiment.

Cyclic steps can occur in net-erosional (Parker and Izumi, 2000) or net-depositional flows (Sun and Parker, 2005): Fildani et al. (2006) suggested that the steps in the distributary channel on the Monterey Fan are analogous to the former, whereas fields of sediment waves found throughout the fan are analogous to the latter. From the topographic low of the distributary channel on the Eel Canyon, we know that depositional flows in this region are rare. The fields of sediment waves on the northern lobe, however, could be depositional cyclic steps. The difference in size of the cyclic steps in Eel Canyon compared to the Monterey Fan might be due to differences in the size of the characteristic turbidity currents in the distributary channels (smaller $\mathrm{Fr_d}$ favors larger steps), the erodibility of the bed (more easily erodible material favors larger steps), or the overall channel slope (lower channel slope favors larger steps) (Parker and Izumi, 2000). This latter prediction is consistent with observations. The overall slope in the Eel Canyon distributary channel is ~2.9%, whereas the Monterey Fan distributary has a lower slope ranging from 0.3% to 1.3% (Fildani et al., 2006), and has larger steps.

Despite the uncertainty in the role of tectonics in regulating the depth and history of the distributary, the location of the distributary head is likely a result of tectonic activity. The oblique compressional tectonics has had a tendency to juxtapose different reaches of the canyon. Where margin-parallel perturbations become too large, turbidity currents can migrate because of the propensity of these flows to superelevate. Targeted multichannel seismic imaging of the canyon may help resolve the relative strengths of turbidity-current incision and tectonic deformation.

Another interesting problem motivating future exploration of the canyon is determination of the percentage of flow that exits the canyon via the distributary. Such an analysis is difficult because only rough estimates for the sizes of flows can be determined. A controversial idea is that the distributary could be an indication of avulsion and abandonment of the main canyon. If ignitive flows (i.e., flows that are able to erode a considerable amount of material along their path and thus become significantly larger than the original event) are common, their size may be sufficient to propel most of the material outside of the canyon. If incision of the distributary channel outpaces tectonic deformation, the distributary may become an increasingly important pathway of abyssal-bound sediment, reinforcing the avulsion of the main canyon. This could lead to complex patterns in the depositional record, including interfingering turbidite beds and fan lobes, offset stacking of channel-levee complexes (Weimer,

1991; Twichell et al., 1991), and a shift in the depocenter of Eel River sediment.

CONCLUSIONS

The oblique compressional tectonics of the Eel continental margin have forced a significant bend in the submarine Eel Canyon. A distributary channel extends from the canyon rim, at the bend in the canyon, to a northern lobe of the Eel Fan. We have interpreted features within the channel to be cyclic-step bedforms generated by Froude-supercritical turbidity currents. Measurements from cores taken in the upper canyon heads indicate that 2–3 m of predominantly fine-grained sediment fails on decadal time scales (Mullenbach and Nittrouer, 2006). Failure of this material provides the simplest explanation for turbidity currents in the canyon. We propose that the bend in the canyon acts as an obstruction to turbidity currents, forcing them to superelevate and partially overflow the 280-m-high outerbank canyon wall. Our calculations indicate that turbidity currents generated from these failures are capable of partially overflowing the canyon, and that the overflow portion is competent to suspend sand and form the cyclic steps. Superelevation of turbidity currents and channel formation are potentially important processes in the Eel Canyon for shifting the depocenter of Eel River sediments through a partial avulsion of the canyon. Such processes might be important on other continental margins where tectonics can alter the course of a submarine canyon.

APPENDIX 1 – NOTATION

C	Depth-averaged volumetric sediment concentration
c_f	Bulk friction coefficient
f	Fraction of a failed mass that becomes a turbidity current
Fr_d	Bulk densimetric Froude number
g	Acceleration due to gravity
h	Flow depth
H	Total run-up height
R	Submerged specific density of sediment
S	Average channel slope
u_*	Bed shear velocity
U	Depth-averaged velocity
w_s	Terminal settling velocity of sediment
η	Thickness of a failed mass
ϕ	Porosity of the seabed

ACKNOWLEDGMENTS

This study was funded by Office of Naval Research grant N000149910028 and National Undersea Research Program grant UAF(WA-00–05). Norman Maher helped plan the bathymetric survey. We thank Wayne McCool, John Crockett, David Drake, and Leda Beth Gray for assisting on the cruise. Rob Hagg helped ensure the success in later stages of the cruise by supplying us with on-the-fly imagery of the canyon. Tina Lomnicky aided in post-processing of the multibeam data. Paul Heller, Roger Slatt, John Warme, and Gerilyn Soreghan provided helpful reviews of an earlier draft. Paul Heller and Carlos Pirmez provided constructive reviews of this manuscript. Gary Parker inspired our interpretation of the cyclic steps.

REFERENCES CITED

Alexander, C.R., and Simoneau, A.M., 1999, Spatial variability in sedimentary processes on the Eel continental slope: Marine Geology, v. 154, p. 243–254, doi: 10.1016/S0025-3227(98)00116-9.

Atwater, T., 1970, Implications of plate tectonics for the Cenozoic tectonic evolution of western North America: Geological Society of America Bulletin, v. 81, p. 3513–3536, doi: 10.1130/0016-7606(1970)81[3513:IOPTFT]2.0.CO;2.

Burger, R.L., Fulthrope, C.S., and Austin, J.A., 2001, Late Pleistocene channel incisions in the southern Eel River Basin, northern California: Implications for tectonic vs. eustatic influences on shelf sedimentation patterns: Marine Geology, v. 177, p. 317–330, doi: 10.1016/S0025-3227(01)00166-9.

Burger, R.L., Fulthrope, C.S., Austin, J.A., and Gulick, S.P.S., 2002, Lower Pleistocene to present structural deformation and sequence stratigraphy of the continental shelf, offshore Eel River Basin, northern California: Marine Geology, v. 185, p. 249–281, doi: 10.1016/S0025-3227(02)00196-2.

Clarke, S.H., 1992, Geology of the Eel River basin and adjacent region: Implications for the late Cenozoic tectonics of the southern Cascadia subduction zone and Mendocino triple junction: American Association of Petroleum Geologists Bulletin, v. 76, p. 199–224.

Crockett, J.S., and Nittrouer, C.A., 2004, The sandy inner shelf as a repository for muddy sediment: An example from northern California: Continental Shelf Research, v. 24, p. 55–73, doi: 10.1016/j.csr.2003.09.004.

Dade, W.B., Lister, J.R., and Huppert, H.E., 1994, Fine-sediment deposition from gravity surges on uniform slopes: Journal of Sedimentary Research, ser. A, Sedimentary Petrology and Processes, v. 64, no. 3, p. 423–432.

Daly, R.A., 1936, Origin of submarine canyons: American Journal of Science, v. 31, p. 853–862.

Dietrich, W.E., 1982, Settling velocity of natural particles: Water Resources Research, v. 18, p. 1615–1626.

Drexler, T.D., Nittrouer, C.A., and Mullenbach, B.L., 2006, Impact of local morphology on sedimentation in Eel submarine Canyon: Journal of Sedimentary Research, v. 76, doi: 10.2110/jsr.2006.064.

Driscoll, N.W., Weissel, J.K., and Goff, J.A., 2000, Potential for large-scale submarine slope failure and tsunami generation along the U.S. Mid-Atlantic coast: Geology, v. 28, p. 407–410, doi: 10.1130/0091-7613(2000)28<407:PFLSSF>2.0.CO;2.

Edwards, D.A., 1993, Turbidity currents: Dynamics, deposits and reversals: Springer-Verlag, Lecture Notes in Earth Sciences, v. 44, 175 p.

Fildani, A., and Normark, W.R., 2004, Late Quaternary evolution of channel and lobe complexes of Monterey Fan: Marine Geology, v. 206, p. 199–223, doi: 10.1016/j.margeo.2004.03.001.

Fildani, A., Normark, W.R., Kostic, S., and Parker, G., 2006, Channel formation by flow stripping: Large-scale scour features along the Monterey East Channel and their relation to sediment waves: Sedimentology, v. 53, p. 1265–1287, doi: 10.1111/j.1365-3091.2006.00812.x.

Goff, J.A., Mayer, L.A., Hughes-Clarke, J., and Pratson, L.F., 1996, Swath mapping on the continental shelf and slope: The Eel River Basin, northern California: Oceanography, v. 9, p. 178–182.

Greene, H.G., Maher, N.M., and Paull, C.K., 2002, Physiography of the Monterey Bay National Marine Sanctuary and implications about continental margin development: Marine Geology, v. 181, p. 55–82, doi: 10.1016/S0025-3227(01)00261-4.

Griggs, G.B., and Hein, J.R., 1972, Sources, dispersal and clay-mineral composition of fine-grained sediment off of central and northern California: Journal of Geology, v. 88, p. 541–566.

Gulick, S.P.S., and Meltzer, A.S., 2002, Effect of the northward-migrating Mendocino triple junction on the Eel River forearc basin, California: Structural evolution: Geological Society of America Bulletin, v. 114, p. 1505–1519, doi: 10.1130/0016-7606(2002)114<1505:EOTNMM>2.0.CO;2.

Gulick, S.P.S., Meltzer, A.S., and Clarke, S.H., 1998, Seismic structure of the southern Cascadia subduction zone and accretionary prism north of the Mendocino triple junction: Journal of Geophysical Research, v. 103, p. 27,207–27,222, doi: 10.1029/98JB02526.

Gulick, S.P.S., Meltzer, A.S., and Clarke, S.H., 2002, Effect of the northward-migrating Mendocino triple junction on the Eel River forearc basin, California: Stratigraphic development: Geological Society of America Bulletin, v. 114, p. 178–191, doi: 10.1130/0016-7606(2002)114<0178:EOTNMM>2.0.CO;2.

Hagen, R.A., Vergara, H., and Naar, D.F., 1996, Morphology of San Antonio submarine canyon on the central Chile forearc: Marine Geology, v. 129, p. 197–205, doi: 10.1016/0025-3227(96)83345-7.

Hay, A.E., 1987, Turbidity currents and submarine channel formation in Rupert Inlet, British Columbia: 1. Surge observations: Journal of Geophysical Research, v. 92, p. 2875–2881.

Heezen, B.C., and Ewing, W.M., 1952, Turbidity currents and submarine slumps, and the 1929 Grand Banks earthquake: American Journal of Science, v. 250, p. 849–873.

Inman, D.L., Nordstrom, and Flick, R.E., 1976, Currents in submarine canyons: An air-sea-land interaction: Annual Review of Fluid Mechanics, v. 8, p. 275–310.

Jenson, S.K., and Domingue, J.O., 1988, Extracting topographic structure from digital elevation data for geographic information systems analysis: Photogrammetric Engineering and Remote Sensing, v. 54, p. 1593–1600.

Johnson, K.S., Paull, C.K., Barry, J.P., and Chavez, F.P., 2001, A decadal record of underflows from a coastal river into the deep sea: Geology, v. 29, p. 1019–1022, doi: 10.1130/0091-7613(2001)029<1019:ADROUF>2.0.CO;2.

Kineke, G.C., Woolfe, K.J., Kuehl, S.A., Milliman, J.D., Dellapenna, T.M., and Purdon, R.G., 2000, Sediment export from the Sepik River, Papua New Guinea: Evidence for a divergent sediment plume: Continental Shelf Research, v. 20, p. 2239–2266, doi: 10.1016/S0278-4343(00)00069-8.

Kneller, B., and Buckee, C., 2000, The structure and fluid mechanics of turbidity currents: A review of some recent studies and their geological implications: Sedimentology, v. 47, p. 62–94, doi: 10.1046/j.1365-3091.2000.047s1062.x.

Kneller, B.C., and McCaffrey, W.D., 1999, Depositional effects of flow non-uniformity and stratification within turbidity currents approaching a bounding slope: Deflection, reflection and facies variation: Journal of Sedimentary Research, v. 69, p. 980–991.

Komar, P.D., 1969, The channelized flow of turbidity currents with application to Monterey Deep-Sea Channel: Geological Society of America Bulletin, v. 79, p. 4544–4558.

Kostic, S., and Parker, G., 2006, The response of turbidity currents to a canyon-fan transition: Internal hydraulic jumps and depositional signatures: Journal of Hydraulic Research, v. 44, p. 631–653.

Koyama, T., and Ikeda, H., 1998, Effect of riverbed gradient on bedrock channel configuration: A flume experiment: Proceedings of the Environmental Research Center, Tsukuba University, Japan, v. 23, p. 25–34.

Kuenen, P.H., 1937, Experiments in connection with Daly's hypothesis on the formation of submarine canyons: Leidsche Geolgische Mededeelingen, v. 8, p. 316–351.

Lamb, M.P., and Parsons, J.D., 2005, High-density suspensions formed under waves: Journal of Sedimentary Research, v. 75, p. 386–397, doi: 10.2110/jsr.2005.030.

Lamb, M.P., Hickson, T., Marr, J.G., Sheets, B., Paola, C., and Parker, G., 2004a, Surging vs. continuous turbidity currents: Flow dynamics and deposits in an experimental intraslope minibasin: Journal of Sedimentary Research, v. 74, p. 148–155.

Lamb, M.P., D'Asaro, E., and Parsons, J.D., 2004b, Turbulent structure of high-density suspensions formed

under waves: Journal of Geophysical Research, v. 109, C121026, doi: 10.1029/2004JV002355.

Lamb, M.P., Toniolo, H., and Parker, G., 2006, Trapping of sustained turbidity currents by intraslope minibasins: Sedimentology, v. 53, p. 147–160, doi: 10.1111/j.1365-3091.2005.00754.x.

Lane-Serff, G.F., Beal, L.M., and Hadfield, T.D., 1995, Gravity current flow over obstacles: Journal of Fluid Mechanics, v. 292, p. 39–54, doi: 10.1017/S002211209500142X.

Marr, J.G., Harff, P.A., Shanmugam, G., and Parker, G., 2001, Experiments on subaqueous sandy gravity flows: The role of clay and water content in flow dynamics and depositional structures: Geological Society of America Bulletin, v. 113, p. 1377–1386, doi: 10.1130/0016-7606(2001)113<1377:EOSSGF>2.0.CO;2.

Martz, L.W., and Garbrecht, W.P., 1998, The treatment of flat areas and depressions in automated drainage analysis of raster digital elevation models: Hydrological Processes, v. 12, p. 843–855, doi: 10.1002/(SICI)1099-1085(199805)12:6<843::AID-HYP658>3.0.CO;2-R.

McCrory, P.A., 1989, Late Neogene geohistory analysis of the Humboldt Basin and its relationship to convergence of the Juan de Fuca Plate: Journal of Geophysical Research, v. 94, no. B3, p. 3126–3138.

Milliman, J.D., and Syvitski, J.P.M., 1992, Geomorphic/tectonic control of sediment discharge to the ocean: the importance of small mountain rivers: Geology, v. 100, p. 525–544.

Mohrig, D., and Marr, J.G., 2003, Constraining the efficiency of turbidity current generation from submarine debris flows and slides using laboratory experiments: Marine and Petroleum Geology, v. 20, p. 883–899, doi: 10.1016/j.marpetgeo.2003.03.002.

Mohrig, D., Whipple, K.X., Hondzo, M., Ellis, C., and Parker, G., 1998, Hydroplaning of subaqueous debris flows: Geological Society of America Bulletin, v. 110, p. 387–394, doi: 10.1130/0016-7606(1998)110<0387:HOSDF>2.3.CO;2.

Muck, M.Y., and Underwood, M.B., 1990, Upslope flow of turbidity currents: A comparison among field observations, theory, and laboratory methods: Geology, v. 18, p. 54–57, doi: 10.1130/0091-7613(1990)018<0054:UFOTCA>2.3.CO;2.

Mulder, T., and Syvitski, J.P.M., 1995, Turbidity currents generated at river mouths during exceptional discharges to the world oceans: Journal of Geology, v. 103, p. 285–299.

Mulder, T., Savoye, B., Syvitski, J.P.M., and Parize, O., 1997, Hyperpycnal turbidity currents at the head of the Var Canyon? Hydrological data and geological observations: Oceanologica Acta, v. 20, p. 607–626.

Mullenbach, B.L., and Nittrouer, C.A., 2006, Decadal record of sediment export to the deep sea via Eel Canyon: Continental Shelf Research, v. 26, p. 2157–2177, doi: 10.1016/j.csr.2006.07.019.

Mullenbach, B.L., Nittrouer, C.A., and Puig, P., 2004, Sediment deposition in a modern submarine canyon: Eel Canyon, northern California: Marine Geology, v. 211, p. 101–119, doi: 10.1016/j.margeo.2004.07.003.

Myrow, P.M., Lamb, M.P., Lukens, C., and Houck, K., 2006, Paleohydraulic interpretations of wave-modified hyperpycnal flow deposits: Eos (Transactions, American Geophysical Union), v. 87, Fall Meeting Supplement, abs. PP23B-1763.

Nelson, C.H., Goldfinger, C., Johnson, J.E., and Dunhill, G., 2000, Variation of modern turbidite systems along the subduction zone margin of Cascadia Basin and implications for turbidite reservoir beds: Houston, GCSSEPM Foundation 20th Annual Research Conference Proceedings, p. 714–738.

Nemec, W., 1995, The dynamics of deltaic suspension plumes, *in* Oti, M.N., and Postma, G., eds., Geology of deltas: Rotterdam, A.A. Balkema, p. 31–93.

Nittrouer, C.A., 1999, STRATAFORM: Overview of its design and synthesis of its results: Marine Geology, v. 154, p. 3–12, doi: 10.1016/S0025-3227(98)00128-5.

Nittrouer, C.A., and Kravitz, J.H., 1996, STRATAFORM: A program to study the creation and interpretation of sedimentary strata on continental margins: Oceanography, v. 9, p. 146–152.

Nittrouer, C.A., Austin, J.A., Jr., Field, M.E., Kravitz, J.H., Syvitski, J.P.M., and Wiberg, P.L., eds., 2007, Continental-margin sedimentation: From sediment transport to sequence stratigraphy: International Association of Sedimentologists Special Publication 37, 549 p.

Normark, W.R., Posamentier, H., and Mutti, E., 1993, Turbidite systems: State of the art and future directions: Reviews of Geophysics, v. 31, p. 91–116, doi: 10.1029/92RG02832.

Ogston, A.S., Cacchione, R., Sternberg, W., and Kineke, G.C., 2000, Observations of storm and river flood-driven sediment transport on the northern California continental shelf: Continental Shelf Research, v. 20, p. 2141–2162, doi: 10.1016/S0278-4343(00)00065-0.

Orange, D.L., 1999, Tectonics, sedimentation, and erosion in northern California: Submarine geomorphology and sediment preservation potential as a result of three competing processes: Marine Geology, v. 154, p. 369–382, doi: 10.1016/S0025-3227(98)00124-8.

Parker, G., 1982, Conditions for the ignition of catastrophically erosive turbidity currents: Marine Geology, v. 46, p. 307–327, doi: 10.1016/0025-3227(82)90086-X.

Parker, G., and Izumi, N., 2000, Purely erosional cyclic and solitary steps created by flow over a cohesive bed: Journal of Fluid Mechanics, v. 419, p. 203–238, doi: 10.1017/S0022112000001403.

Parker, G., Fukushima, Y., and Pantin, H.M., 1986, Self-accelerating turbidity currents: Journal of Fluid Mechanics, v. 171, p. 145–181, doi: 10.1017/S0022112086001404.

Parker, G., Garcia, M., Fukushima, Y., and Yu, W., 1987, Experiments on turbidity currents over an erodible bed: Journal of Hydraulic Research, v. 25, p. 123–147.

Parsons, J.D., and Garcia, M.H., 1998, Similarity of gravity current fronts: Physics of Fluids, v. 10, p. 3209–3213, doi: 10.1063/1.869848.

Parsons, J.D., Bush, J.W.M., and Syvitski, J.W.M., 2001, Hyperpycnal plumes with small sediment concentrations: Sedimentology, v. 48, p. 465–478, doi: 10.1046/j.1365-3091.2001.00384.x.

Parsons, J.D., Friedrichs, C.T., Traykovski, P.A., Mohrig, D., Imran, J., Syvitski, J.P.M., Parker, G., and Puig, P., Buttles, J.L. and Garcia, M.H., 2007, The mechanics of marine sediment gravity flows, *in* Nittrouer, C.A., et al., eds., Continental-margin sedimentation: From sediment transport to sequence stratigraphy: International Association of Sedimentologists Special Publication 37, p. 275–337.

Paull, C.K., Ussler, W., Greene, H.G., Keaten, R., Mitts, P., and Barry, J., 2003, Caught in the act: The 20 December 2001 gravity flow event in Monterey Canyon: Geo-Marine Letters, v. 22, p. 227–232, doi: 10.1007/s00367–003–0117–2.

Peakall, J., McCaffrey, B., and Kneller, B., 2000, A process model for the evolution, morphology, and architecture of sinuous submarine channels: Journal of Sedimentary Research, v. 70, p. 434–448.

Pirmez, C., and Imran, J., 2003, Reconstruction of turbidity currents in Amazon Channel: Marine and Petroleum Geology, v. 20, p. 823–849, doi: 10.1016/j.marpetgeo.2003.03.005.

Posamentier, H.W., Erksine, R.D., and Mitchum, R.M., 1991, Models for submarine fan deposition within a sequence stratigraphic framework, *in* Weimer, P., and Link, M.H., eds., Seismic facies and sedimentary processes of submarine fans and turbidite systems: Berlin, Springer, p. 127–136.

Pratson, L.F., and Ryan, W.B.F., 1994, Pliocene to recent infilling and subsidence of intraslope basins offshore Louisiana: American Association of Petroleum Geologists Bulletin, v. 78, p. 1483–1506.

Puig, P., Ogston, A.S., Mullenbach, B.L., Nittrouer, C.A., and Sternberg, R.W., 2003, Shelf-to-canyon sediment-transport processes on the Eel continental margin (northern California): Marine Geology, v. 193, p. 129–149, doi: 10.1016/S0025-3227(02)00641-2.

Puig, P., Ogston, A.S., Mullenbach, B.L., Nittrouer, C.A., and Parsons, J.D., 2004, Storm-induced sediment gravity flows at the head of the Eel submarine canyon, northern Californian Margin: Journal of Geophysical Research, v. 109, C03019, doi: 10.1029/2003JC001918.

Rottman, J.W., Simpson, J.E., and Hunt, J.C.R., 1985, Unsteady gravity current flows over obstacles: some observations and analysis related to the Phase II trials: Journal of Hazardous Materials, v. 11, p. 325–340, doi: 10.1016/0304-3894(85)85044-5.

Sawai, K., 1977, Sediment hydraulics research on the mechanism of variation of the bed of cohesive channels [Ph.D. thesis]: Kyoto, Japan, Kyoto University (in Japanese).

Scully, M.E., Friedrichs, C.T., and Wright, L.D., 2003, Numerical modeling of gravity-driven sediment transport and deposition on an energetic continental shelf: Eel River, northern California: Journal of Geophysical Research—Oceans, v. 108, no. C4, 3120, doi: 10.1029/2002JC001467.

Shepard, F.P., and Dill, R.F., 1966, Submarine canyons and other sea valleys: Chicago, Illinois, Rand McNally, 381 p.

Sommerfield, C.K., and Nittrouer, C.A., 1999, Modern accumulation rates and a sediment budget for the Eel shelf: A flood-dominated depositional environment: Marine Geology, v. 154, p. 227–241, doi: 10.1016/S0025-3227(98)00115-7.

Stow, D.A.V., Howell, D.G., and Nelson, C.H., 1985, Sedimentary, tectonic, and sea-level controls, *in* Bouma, A.H., et al., eds., Submarine fans and related turbidite systems: New York, Springer, p. 15–22.

Straub, K.M., Mohrig, D.C., Buttles, J., McElroy, B., and Pirmez, C., 2008, Interactions between turbidity currents and topography in aggrading sinuous submarine channels: A laboratory study: Geological Society of America Bulletin (in press).

Sun, T., and Parker, G., 2005, Transportational cyclic steps created by flow over an erodible bed. Part 2. Theory and numerical simulation: Journal of Hydraulic Research, v. 43, p. 502–514.

Taki, K., and Parker, G., 2005, Transportational cyclic steps created by flow over an erodible bed. Part 1. Experiments: Journal of Hydraulic Research, v. 43, p. 488–501.

Traykovski, P., Geyer, W.R., Irish, J.D., and Lynch, J.F., 2000, The role of wave-induced density-driven fluid mud flows for cross-shelf transport on the Eel River continental shelf: Continental Shelf Research, v. 20, p. 2113–2140, doi: 10.1016/S0278-4343(00)00071-6.

Twichell, D.C., Kenyon, N.H., Parson, L.M., and McGregor, B.A., 1991, Depositional patterns of the Mississippi fan surface: Evidence for Gloria II and high-resolution seismic profiles, *in* Weimer, P., and Link, M.H., eds., Seismic facies and sedimentary processes of submarine fans and turbidite systems: Berlin, Springer, p. 349–364.

Walsh, J.P., and Nittrouer, C.A., 2003, Contrasting styles of off-shelf sediment accumulation in New Guinea: Marine Geology, v. 196, p. 105–125, doi: 10.1016/S0025-3227(03)00069-0.

Weimer, P., 1991, Seismic facies, characteristics, and variations in channel evolution, Mississippi fan (Plio-Pleistocene), Gulf of Mexico, *in* Weimer, P., and Link, M.H., eds., Seismic facies and sedimentary processes of submarine fans and turbidite systems: Berlin, Springer, p. 323–348.

Wheatcroft, R.A., and Borgeld, J.C., 2000, Oceanic flood deposits on the northern California shelf: Large-scale distribution and small-scale physical properties: Continental Shelf Research, v. 20, p. 2163–2190, doi: 10.1016/S0278-4343(00)00066-2.

Wohl, E.E., 2000, Substrate influences on step-pool sequences in Christopher Creek drainage, Arizona: Geology, v. 108, p. 121–129, doi: 10.1086/314385.

Manuscript Received 23 January 2007
Revised Manuscript Received 19 July 2007
Manuscript Accepted 29 August 2007

Printed in the USA